From Large to Small Polarons in Lead, Tin and Mixed Lead-Tin Halide Perovskites

Arup Mahata,[a,b*] Daniele Meggiolaro,[a,b*] , Filippo De Angelis [a,b,c]

[a]Computational Laboratory for Hybrid/Organic Photovoltaics (CLHYO), Istituto CNR di Scienze

e Tecnologie Molecolari (ISTM-CNR), Via Elce di Sotto 8, 06123, Perugia, Italy.

[b]CompuNet, Istituto Italiano di Tecnologia, Via Morego 30, 16163 Genova, Italy.

[c] Department of Chemistry, Biology and Biotechnology, University of Perugia, Via Elce di Sotto

8, 06123, Perugia, Italy.

Abstract

The origin of the long carrier-lifetime in Lead halide perovskites is still under debate and, among different hypothesis, the formation of large polarons preventing the recombination of charge couples is one of the most fascinating. In this work, using state of the art ab initio calculations, we report a systematic study of the polaron formation process in metal halides perovskites focusing on the influence of the chemical composition of the perovskite on the polaron properties. We examine variations in A-site cations (FA, MA, Cs and Cs:MA), B-site cations (Pb, Sn and Pb:Sn) and X-site anions (Br, I). Our study confirms the stronger structural distortions occur for Cs than for MA and FA, with the effect of different A-site cations being almost additive. For the same A-cation, bromide features stronger distortions than iodide perovskites. The pure Sn phase has an almost double polaron stabilization energy than the pure Pb phase. Surprisingly, the trend of polaron stabilization energy is non monotonic in mixed Sn:Pb perovskites, with a maximum for small Sn percentages. Polaron formation is found to be promoted by bond asymmetry, ranging from small to large polarons in mixed Sn:Pb perovskites depending on the relative Sn percentage.

TOC:

50 % Sn   3 % Sn

Large Polaron   **Small Polaron**
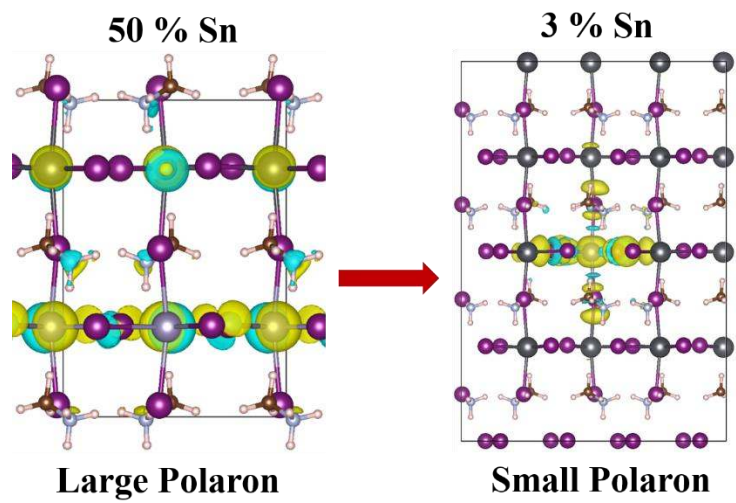
Metal halide perovskites with chemical formula ABX_3, where A= monocation, B= dication and X= halide, have gained great interest as very promising materials for efficient solar cells.[1] These materials provide high power conversion efficiencies in solar cell devices due to a direct band gap with an associated large absorption cross section,[2, 3] and to low recombination rates of the photo-generated charge carriers. Very long lifetimes and diffusion paths of electrons and holes are reported in this class of materials, even in presence of moderately high densities of defects in the lattice, coupled to high carriers mobilities.[4-8] The origin of the low electron-hole recombination rate is still under debate and multiple possibilities have been proposed by the community, e.g. Rashba effect,[9, 10] a ferroelectric behavior[11-13], or the formation of large polarons.[14, 15] The Rashba effect is the splitting of VB and CB of the perovskite into two bands laterally separated in momentum and in energy due to spin-orbit coupling, particularly relevant for the heavy Pb and I nuclei. This leads to a change of the band gap from direct to indirect, by partially suppressing the radiative recombination rate of the photo-generated carriers.[9, 16, 17] On the other hand, formation of ferroelectric domains may promote the spatial separation of electrons and holes, thus lowering the spatial overlap and the carrier recombination rate.[11, 12] Formation of polarons has also been proposed to explain the low recombination rates of charge carriers in lead-halide perovskites.[14, 15] Due to the soft nature of the lattice, photo-generated charge carriers can couple to polar optical phonons by generating polarons. In this process the free carriers are stabilized by, and accommodate a local lattice distortion induced by the optical phonon. The electron–phonon coupling strength determines both the binding energy and the spatial extension of the polaron.[18] Few previous studies have attempted to explain the nature of polarons and their binding energy in 3D [15, 19-22] as well as in 2D and 0D perovskites.[23-25] In a previous work, by a combined experimental-theoretical work based on optical Kerr effects

experiments and hybrid functional Density Functional Theory (DFT), some of us showed that in lead halide perovskites polarons extending over several unit cells can form under photo-excitation.[15] Formation of such 'large polarons' has different implications for carriers dynamics than formation of 'small polarons', commonly encountered in *e.g.* oxides and organics, where the structural distortion occurs locally.[21] Formation of small polarons is usually facilitated by the presence of lattice defects and can activate charge trapping processes with detrimental effects for the carrier transport and overall solar cell device efficiency.[26, 27] On the other hand, formation of large polarons is mostly associated to a bending of the band edges (valence band upshift and conduction band downshift for positive and negative carriers, respectively) while partly retaining the delocalized nature of the free carrier.[28, 29] A different spatial localization of electron and hole polarons in the lattice, associated to opposite structural displacements (*i.e.* a bond compression for a hole and a bond elongation for an electron), [15] is essential to limit the associated recombination rates. Theoretical works based on hybrid DFT-based molecular dynamics confirmed that the coupling of the free charge with the lattice distortion leads to a localization of holes and electrons in different planes of the $MAPbI_3$ perovskite, thus reducing their spatial overlap and recombination probability.[30] In the thermalization process, the polaron phonon cloud get equilibrated by transferring thermal energy to the lattice, leading to a cooled charge carrier state. It has been proposed that the long time decay (>100ps) of hot carriers in halide perovskites can be attributed to the large polaron screening at low excitation density[31-34], whereas at higher excitation densities the cooling of hot phonons is slower and can reheat the electronic degrees of freedom[32, 35, 36] ("phonon-bottleneck") caused by large polaron overlapping.[37] Time-resolved optical Kerr effect spectroscopy estimated large polaron formation times to be around 0.3 ps to 0.7 ps in $MAPbBr_3$ and $CsPbBr_3$ perovskites.[15] Using large-scale ab initio derived tight-binding

model, Zheng et al. reported that the large polaron slows down the electron mobility by roughly a factor of two.[38]

Despite these body of studies little is known about the polaron physics in different perovskites and in particular on the effect of different chemical composition on polaron energetics and spatial distribution. Understanding the role of the organic/inorganic A-site cations on the polaron physics is particularly important in relation to the recent practice of introducing mix-cations in order to increase the stability of the perovskite lattice.[39] On the other hand, the impact of the divalent metal substitution on the B-site is particularly interesting due to the raising interest in mixed Pb-Sn and lead-free perovskites which share similar properties with the most efficient lead-halide perovskites. Longer carrier lifetime[40] and intermediate bandgap between than that of two $APbX_3$ and $ASnX_3$ end compositions [41-46] in mixed Pb-Sn perovskites have been reported, with the additional possibility of tuning the associated bandgap by varying the Sn:Pb ratio. This paves the way to the design of novel full perovskites tandem cells.[30] Notably, the notorious instability of Sn-based perovskites can be significantly improved by Pb alloying in mixed compositions.[43, 47-49] Similarly, variations on the X halide are expected to lead to quantitative differences in the response to charges, due to the different energetics and spatial extent of the halide p orbitals. While iodide perovskites are dominating the solar cell literature, bromide perovskites are interesting also for lighting applications.[50-53]

In light of the huge interest in tuning chemical perovskite composition towards specific optoelectronic response, in this work we systematically investigate the nature, spatial extent and energetics of polaron formation in metal halide perovskites by focusing on the effects of A, B and X substitution on the polaron stabilization energy and the resulting coupling with the lattice phonons. Starting from the prototype $MAPbI_3$ perovskite, we have collectively investigated

6

substitution at the A- (Cs → MA → FA), B- (Pb → Sn) and X-sites (I → Br), considering in selected cases mixed phases, such as the A-mixed (Cs/MA)PbI$_3$ and the B-mixed MA(Sn/Pb)I$_3$ perovskites. We find that polaron formation is enhanced by apolar small A-cations (Cs vs. MA and FA) and by lighter X-halides (Br vs. I), with their combined effect being roughly additive. While pure B- perovskites (*e.g.* MAPbI$_3$ and MASnI$_3$) show delocalized large polarons, surprisingly a small polaron emerges in mixed Sn/Pb compositions in the small Sn doping regime. Such small polaron, associated to trapping of photogenerated holes, transforms into a delocalized large polaron upon increasing the Sn:Pb ratio to 50:50. Our results provide a quantitative analysis of carrier/lattice coupling in a wide compositional perovskite range, delivering at the same time the interpretative basis for the associated varying polaron properties.

To quantitatively estimate the response of the lattice to photo-generated charges we have carried out hybrid PBE0[54] functional atomic relaxation of the tetragonal and/or orthorhombic lattice (four formula units, Z=4, with the exception of FAPbI$_3$ where we used a trigonal cell with Z=3) by subtracting and adding one-unit charge to represent the positive and negative polaron, respectively, while keeping fixed the cell parameters to the experimental values (see Text S1 and Table S1 in Supporting Information for details). The use of hybrid functionals is fundamental in order to quantitatively investigate polarons properties in metal halides perovskites. Semi-local functionals, e.g. the PBE functional[55], commonly employed in DFT calculations of solids do not provide an accurate description of the electronic properties of these systems due to self-interaction error.[56, 57] This error is partially corrected by including fractions of exact exchange, as for instance in PBE0 and HSE06 functionals, or by introducing Hubbard corrections as in the DFT+U approach.[58] These methods have been successfully applied to the

study of polarons in oxides and organo-halides perovskites, by showing better accuracies compared to semi-local functionals.[19, 58, 59]

In our calculations we have not included spin-orbit coupling (SOC) effects on the structural relaxation to reduce the computational effort. The inclusion of SOC has a significant impact on the electronic structure of lead halide perovskites leading to a large stabilization of the conduction band (CB) of ~0.8 eV [57] but it has a limited impact, ~0.1 eV, on the valence band (VB) energetics. In order to estimate the effects of the inclusion of SOC on the electrons relaxation energies, we have performed benchmark PBE and PBE-SOC negative relaxations on the MAPbI$_3$ perovskite. Stabilization energies of 9 and 20 meV have been calculated without and with SOC, respectively. This highlights that, although SOC dramatically affects the energy of the CB in perovskites, the effects on the electron polarons stabilization energies are rather limited. On the other hand, the properties of hole polaron are adequately described by our approach due to the more limited effect of SOC on the VB. The polaron binding energy is defined in terms of the relaxation energy following addition of a charge to the optimized geometry of the neutral system. Such relaxation energies monitored for several perovskites of different composition are summarized in Table 1.

Table 1. Polaron stabilization energy for different systems. Some values are replicated in the rows for better understanding the trend.

Systems	Polaron Stabilization Energy (meV)	
	+1	-1
Variations in A-site cations		
MAPbI$_3$	46	6
FAPbI$_3$	47*	5
Cs$_{0.25}$MA$_{0.75}$PbI$_3$	52	9
CsPbI$_3$	96	0
Variations in X-site anion		

MAPbI$_3$	46	6
MAPbBr$_3$	60	10
CsPbBr$_3$	161	10
Variations in B-site cation		
MAPbI$_3$	46	6
MASnI$_3$	75	35
CsSnI$_3$	188	57
Variations in mixed B-site cation		
MAPbI$_3$	46	6
MAPb$_{0.75}$Sn$_{0.25}$I$_3$	155	29
MAPb$_{0.50}$Sn$_{0.50}$I$_3$	97	65
MAPb$_{0.50}$Sn$_{0.50}$I$_3$ -diagonal	92	8
MAPb$_{0.25}$Sn$_{0.75}$I$_3$	80	68
MASnI$_3$	75	35

* the value has been scaled by ¾ to account for the same charge density.

First, we start analyzing results for the prototype tetragonal MAPbI$_3$. We define the polaron stabilization energy as the energy gain adding a charge to the neutral optimized structure and the relaxed optimized structure with the charge, see Scheme 1.
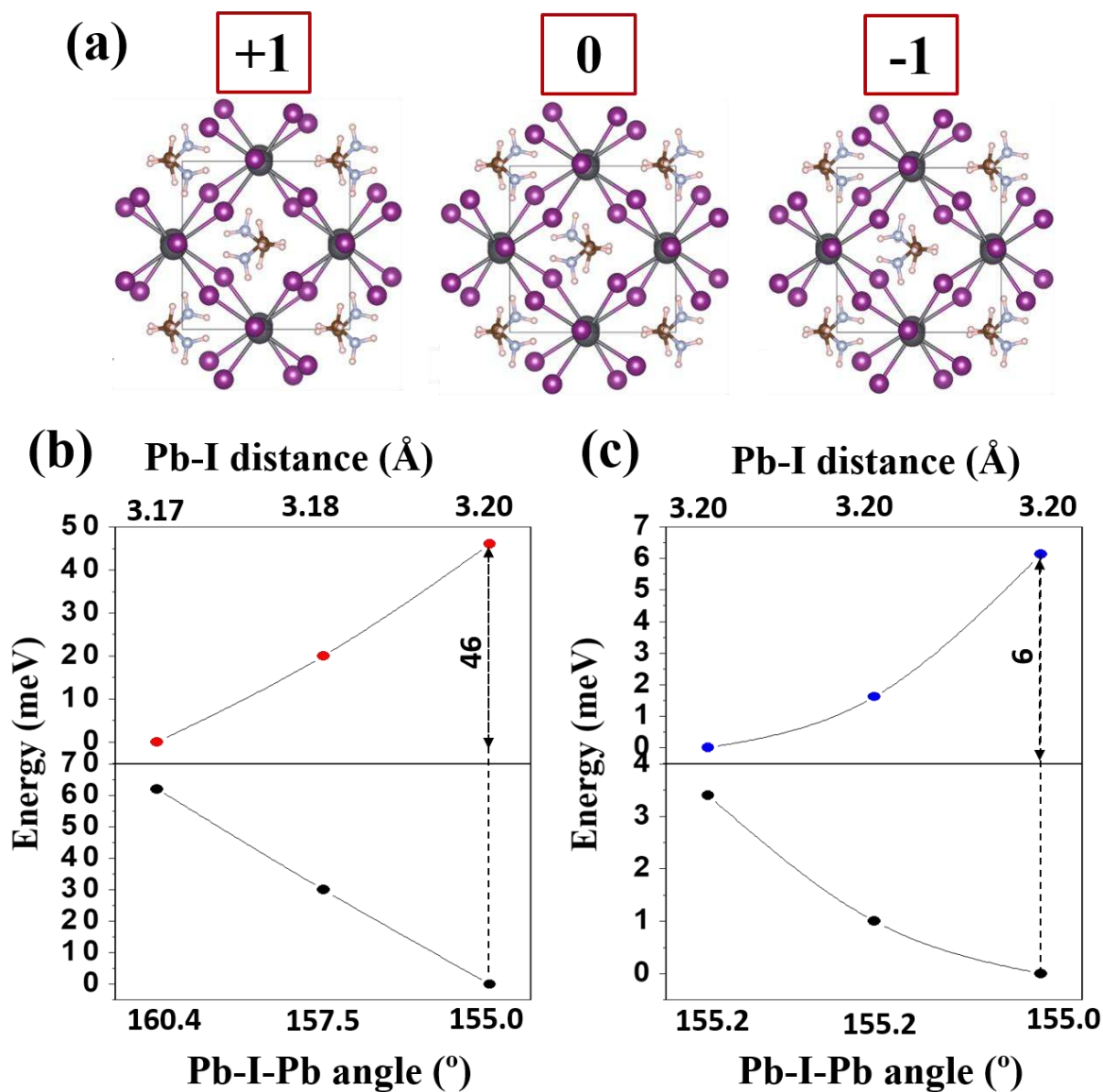
Scheme 1. (A) Relaxed structures of $CH_3NH_3PbI_3$ with positive and negative charge injection. Potential energy surfaces along with structural changes for relaxation of the $CH_3NH_3PbI_3$ upon positive (B; red dot) and negative (C; blue dot) charge injection. The neutral state energy (black dot) along the distortion coordinate is also shown in the bottom panel of (B) and (C).

We find that the hole and electron stabilization energies are 46 and 6 meV, respectively. For all investigated perovskites the relaxation energies induced by the electron are very limited

compared to positive relaxations, see Table 1. Upon hole injection, an average shortening of the Pb-I bond lengths of 0.04 Å and an average reduction of the equatorial Pb-I-Pb bond angle of 5.4° are calculated, in agreement with previous works.[15] The hole injection weakly affects the axial bond lengths and bond angles, see Figure 1.
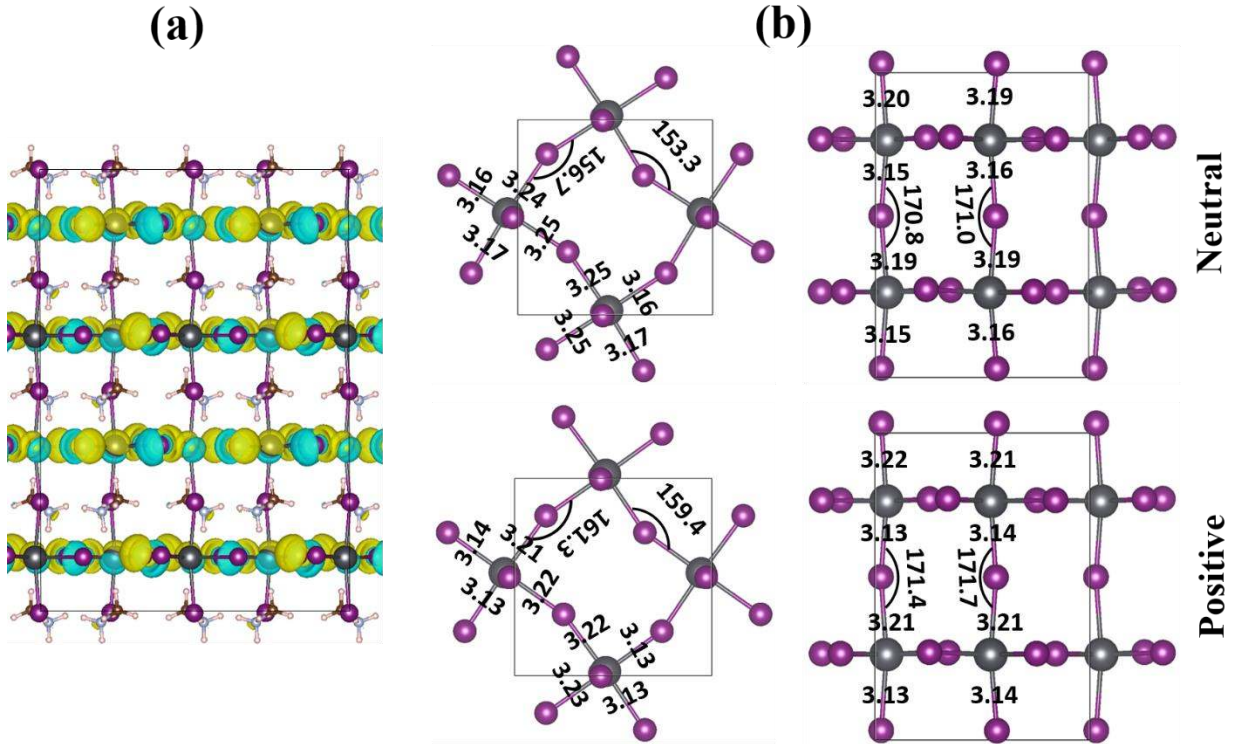

Figure 1. (a) Charge density of hole and (b) structural parameters in neutral and positively charged state of MAPbI$_3$. The two different colors signify the charge accumulation and depletion. Organic Cations have been removed for clarity in the panel (b).

The positive charge delocalizes over all the Pb-I bonds across the lattice, see Figure 1a. To provide a picture of the phonon modes activated by the polaron formation, we have spanned the cartesian lattice relaxation of all ions in the cell induced by the hole over the phonon eigen-displacements calculated at the PBE level for the MAPbI$_3$ perovskite. The coefficients of the spanning procedure reported in the diagram are proportional to the density of phonon modes

activated in the process and are reported, together with the phonon spectrum[60], in Figure 2. The added hole leads to the activation of low energy Pb-I bending and stretching modes below 150 cm^{-1} responsible for the shortening of the Pb-I bonds showed by the structural analysis.
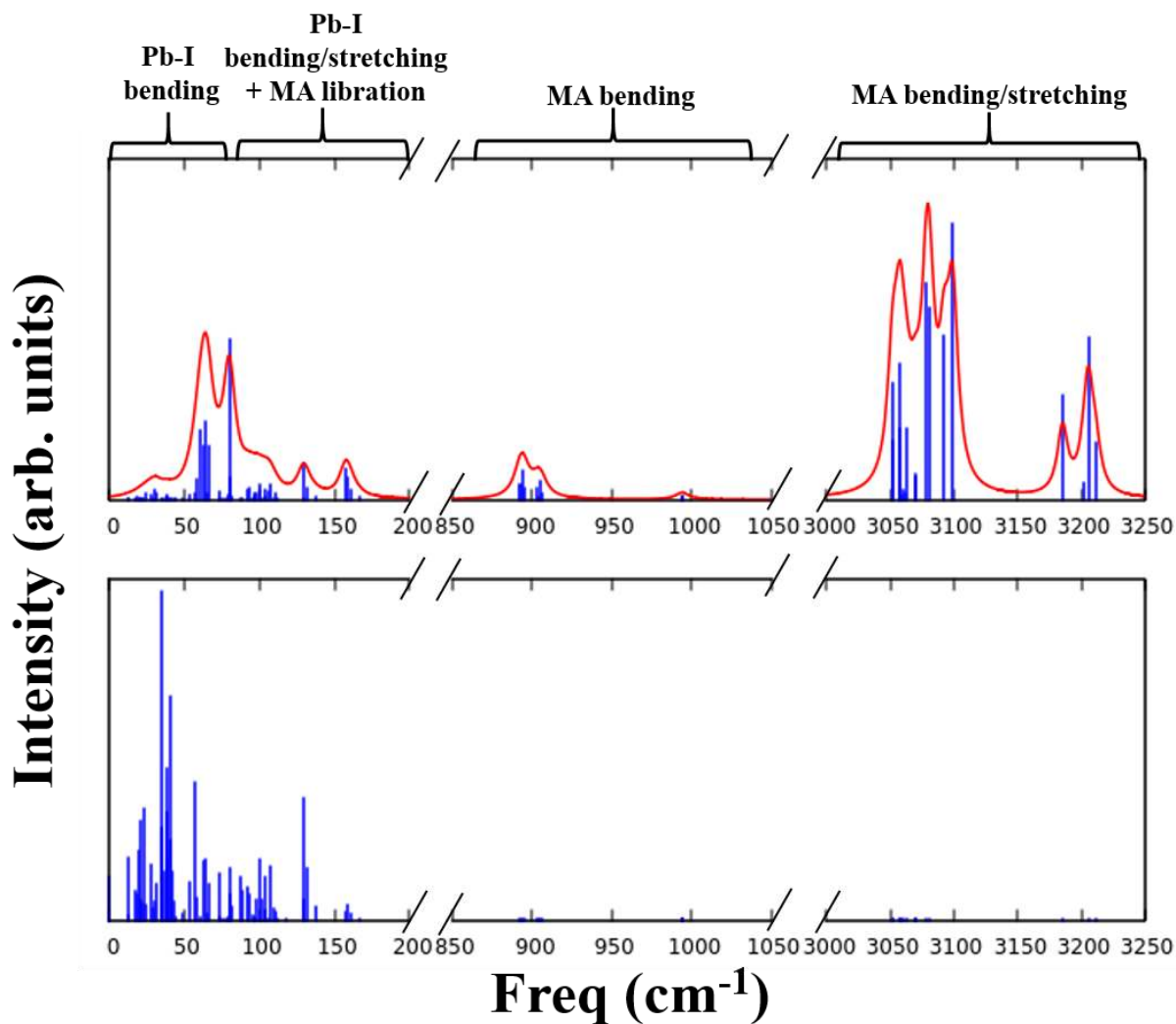

Figure 2. Calculated IR spectrum (top panel) and the coefficients of the displacement vector associated with a positive charge injection (bottom panel) in $MAPbI_3$ projected to the normal modes.

Notice that in our static picture there is very limited contribution of the MA cation vibrational modes to the polaron formation, see Figure 2. Cation reorientation is, however, not captured within a static picture based on geometry optimization but requires a dynamical picture. According to Zhu and coworkers and others, for instance, the A-site organic dipoles can play an active role in the polaron stabilization process due to the screening of the electron–hole Coulomb potential that favors the dissociation of excitons into free carriers, lowering the associated recombination rates.[26, 61, 62] On the other hand, Dastidar et al.[63] and Hutter et al.[64], by studying $CsPbI_3$ and $MAPbI_3$ systems, reported that dipoles have no roles towards the recombination rate and charge carrier mobility, rather fully dominated by the lead iodide framework and emphasized A-site independent factors (*e.g.* Rashba effect) as the reason of slow recombination rates of hybrid perovskites. Using first principle calculations, Kawai et al.[65] investigated the hot-carrier lifetimes from electron-phonon interaction in $MAPbI_3$ and $CsPbI_3$, concluding that the holes decay via the motion of I and Pb ions only, and not the motion of the A-site cation. Ab initio molecular dynamics simulations, however, have shown that the charge-induced relaxation of Pb-I modes is partly assisted by reorientation of the MA cations,[30] confirming a partial role of dipolar cations in stabilizing the polaron formation, though this mainly occurs within the inorganic sub-lattice.

The impact of different A-site cations on the lattice distortion induced by injection of the positive charge is next addressed. We find FA to give rise to the same polaron stabilization than MA, while, in line with previous work on $APbBr_3$ perovskites, Cs has a significantly stronger impact on charge stabilization due to its apolar character not screening added charges.[15] Replacement of one MA-cation of $MAPbI_3$ with Cs, thus modelling the $Cs_{0.25}MA_{0.75}PbI_3$ composition, induces a slight increase of the polaron stabilization energy, in line with the

increase found for the pure $CsPbI_3$ phase, Table 1. The relaxed Pb-I bond lengths of the octahedral of Cs-neighbor of the neutral structure of $CsMAPbI_3$ are 3.12 and 3.17 Å, whereas the same are 3.17 and 3.19 Å in the MA-neighbor octahedral (see Figure S1 in Supporting Information). Therefore, the structure is already distorted in the neutral state. However, upon positive charge injection, the Pb-I bonds get shorter from both type of octahedra by the same extent (0.04 Å), whereas the octahedral distortion is slightly more pronounced in the Cs-octahedra.

By focusing on halide variation, we find that the polaron stabilization energies and the associated structural distortion are larger in bromide than in iodide perovskites. Comparing $APbX_3$ structures, we find a larger hole stabilization energy by 14 and 65 meV for $MAPbBr_3$ and $CsPbBr_3$ compared to $MAPbI_3$ and $CsPbI_3$, see Table 1. This result is somehow expected based on the higher ionization energy of bromide perovskites compared to iodide perovskites, inducing large lattice response to the injection of the charge. The higher electronegativity of Br than I is likely at the origin of the larger distortions reported in bromide perovskites. The higher ionicity of the Pb-Br bond induces a stronger localization of charges associated with higher stabilization energies. Also noticeable is the almost additive effect of changing the A-cation and the X-halide, with $CsPbBr_3$ showing a much stronger coupling to the excess positive charge than $MAPbBr_3$ and $CsPbI_3$.

Then, we move to look to the effect of polaron stabilization by changing the B-site cation. The replacement of Pb by Sn leads to higher polaron stabilization energies independently of the MA or Cs cations, again the effects being almost additive, Table 1. In the case of iodide perovskites, the full Pb replacement by Sn increases the stabilization energies by 29 and 92 meV for $MAPbI_3$ and $CsPbI_3$, respectively. We have then investigated intermediate compositions

modelling the mixed alloys $MAPb_{0.75}Sn_{0.25}I_3$, $MAPb_{0.50}Sn_{0.50}I_3$, $MAPb_{0.25}Sn_{0.75}I_3$. Upon positive charge injection, we find that the structural distortion is more prominent on the equatorial Sn-I bonds for all substituted systems. Most notably, the polaron stabilization energy does not change monotonically by increasing the tin content, but starting from pure $MAPbI_3$ (46 meV) it shows a maximum of 155 meV for $MAPb_{0.75}Sn_{0.25}I_3$ and then it reduces to quite lower values of 97, 80 and 75 meV for $MAPb_{0.50}Sn_{0.50}I_3$, $MAPb_{0.25}Sn_{0.75}I_3$ and $MASnI_3$, respectively. We have rationalized the large polaron stabilization energy of $MAPb_{0.75}Sn_{0.25}I_3$ by looking to its structural relaxation features and the associated electronic structure. In $MAPb_{0.75}Sn_{0.25}I_3$, the four equatorial Sn-I bond distances are 3.00, 3.14, 3.20 and 3.39 Å, which becomes 2.86, 2.93, 3.43 and 3.13 Å, respectively upon positive charge injection. Therefore, there are shortening of two equatorial Sn-I bonds of the octahedra of value 0.14 and 0.21 Å, while the maximum shortening of Pb-I bonds lengths of the same plane is 0.08 Å (central panel of Figure 3b). The shortening of other Pb-I bonds of top layer are negligible (left panel of Figure 3b). The analysis of the projected density of states (PDOS) reported in Figure S2b (Supporting Information) highlights that Pb and Sn along with I contribute to the VBM of $MAPb_{0.75}Sn_{0.25}I_3$. In all substituted systems, however, the electronic states due to Sn are closer in energy to the VBM with respect to the Pb states, in agreement with the lower redox potential of Sn compared to Pb (see Figure S2b-d in Supporting Information). The plot of the VBM Kohn-Sham orbital confirms that the charge density of this state spreads exclusively on the Sn-I-Pb plane, while no charge density is reported on the other two leads in the upper plane (see Figure S3 in Supporting Information). These results suggest that the hole polaron is mainly coupled to deformations of the Sn-I bonds in the lattice and localizes firstly on the Sn-I-Pb plane by leading to a short-long distribution of bonds and allowing a large stabilization. On the other hand, moving from $MAPb_{0.75}Sn_{0.25}I_3$ to

MAPb$_{0.50}$Sn$_{0.50}$I$_3$, the short–long nature (see Figure S4 in Supporting Information) of Sn-I bonds is more limited due to the distribution of the lattice strain over the whole cell. This leads to a diffuse polaron spreading across all metal iodide bonds (see Figure 4c) with a small hole polaron stabilization energy of 97 meV. We have considered two geometries of MAPb$_{0.50}$Sn$_{0.50}$I$_3$; in one case the Sn atoms placed in the same plane and in another case two Sn atoms are placed diagonally. The first case is more stable than the second by 4 meV and 22 meV in GGA and PBE0 level of theory, respectively, with the hole polaron stabilization energy, however, differing by only 5 meV. The different localization of hole polaron in the MAPb$_{0.75}$Sn$_{0.25}$I$_3$ and MAPb$_{0.50}$Sn$_{0.50}$I$_3$ systems highlights that asymmetries in the distribution on bond lengths across different layers lead to preferential polaron 'nucleation' in the layer where shorter metal-halide bonds are present. The equalization of this asymmetry results in a lower localization and stabilization energy of the polaron. This trend proceeds linearly in MAPb$_{0.25}$Sn$_{0.75}$I$_3$ system whose stabilization energy is further reduced to 80 meV, and as expected, also in this case the distortion is mainly localized on the Sn-I bonds, however with small extent (maximum bond shortening of 0.07 and 0.11 Å in the equatorial and axial, respectively) and concomitantly with a delocalization of the polaron density over both planes of the unit cell (see Figure 4d and S5 in Supporting Information). Similarly, in the full replaced MASnI$_3$ system, the Sn-I bonds get shorten throughout the lattice with a maximum shortening of 0.17 and 0.08 Å in the equatorial and axial Sn-I bonds (see Figure S6 in Supporting Information), respectively, and therefore the hole charge density is distributed in all equatorial Sn-I bonds of the lattice (see Figure 4e). Then, it is clear from the above results that the polaron stabilization is mainly influenced by the presence of bond asymmetry, i.e the short-long nature of the metal-halide bond length, with the positive charge mostly accommodating in the short bond lengths region of the lattice. We have

shown that small percentage of Sn-doping creates such structural asymmetry and likely tend to form smaller polarons. To further quantify the nature of small polaron formation in Sn-doped $MAPbI_3$, we have further reduced the Sn-doping concentration to 3 % by considering a $2 \times 2 \times 2$ supercell (with 32 formula units). Interestingly, we find that the hole polaron is formed only at Sn-I bonds and forms a small polaron (see Figure 4a), indicating a possibility of trap states at the Sn-center of lightly Sn-doped $MAPbI_3$.
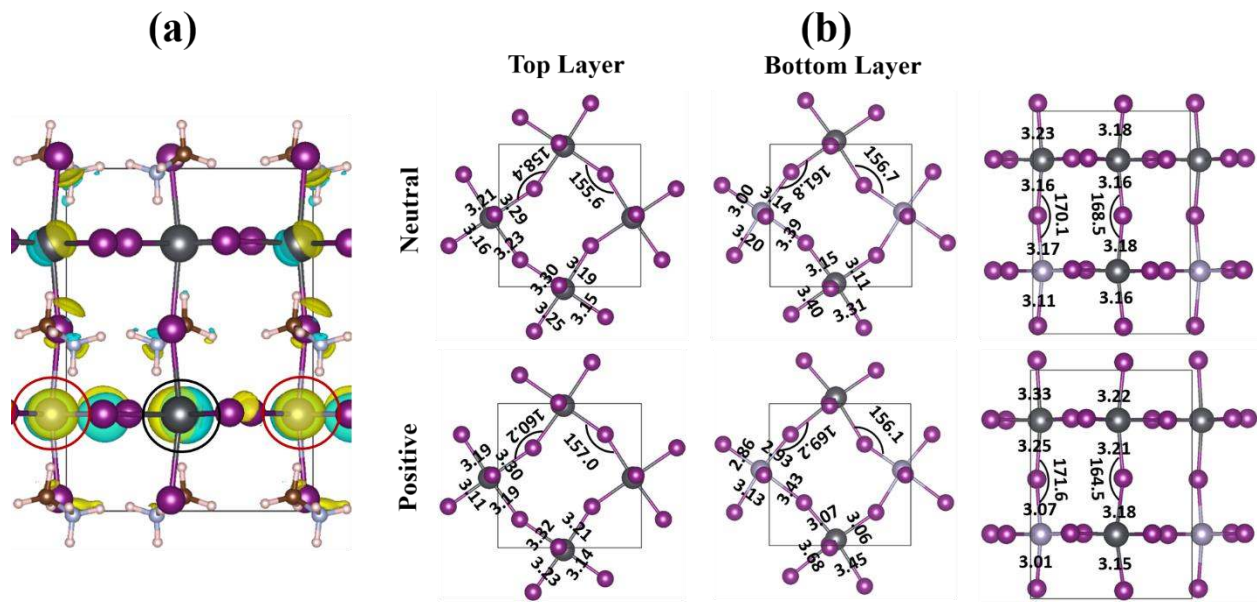

Figure 3: (a) Charge density of hole and (b) structural parameters in neutral and positively charged state of $MAPb_{0.75}Sn_{0.25}I_3$. Highlighted red and black circle represent the Sn and Pb atom, respectively.
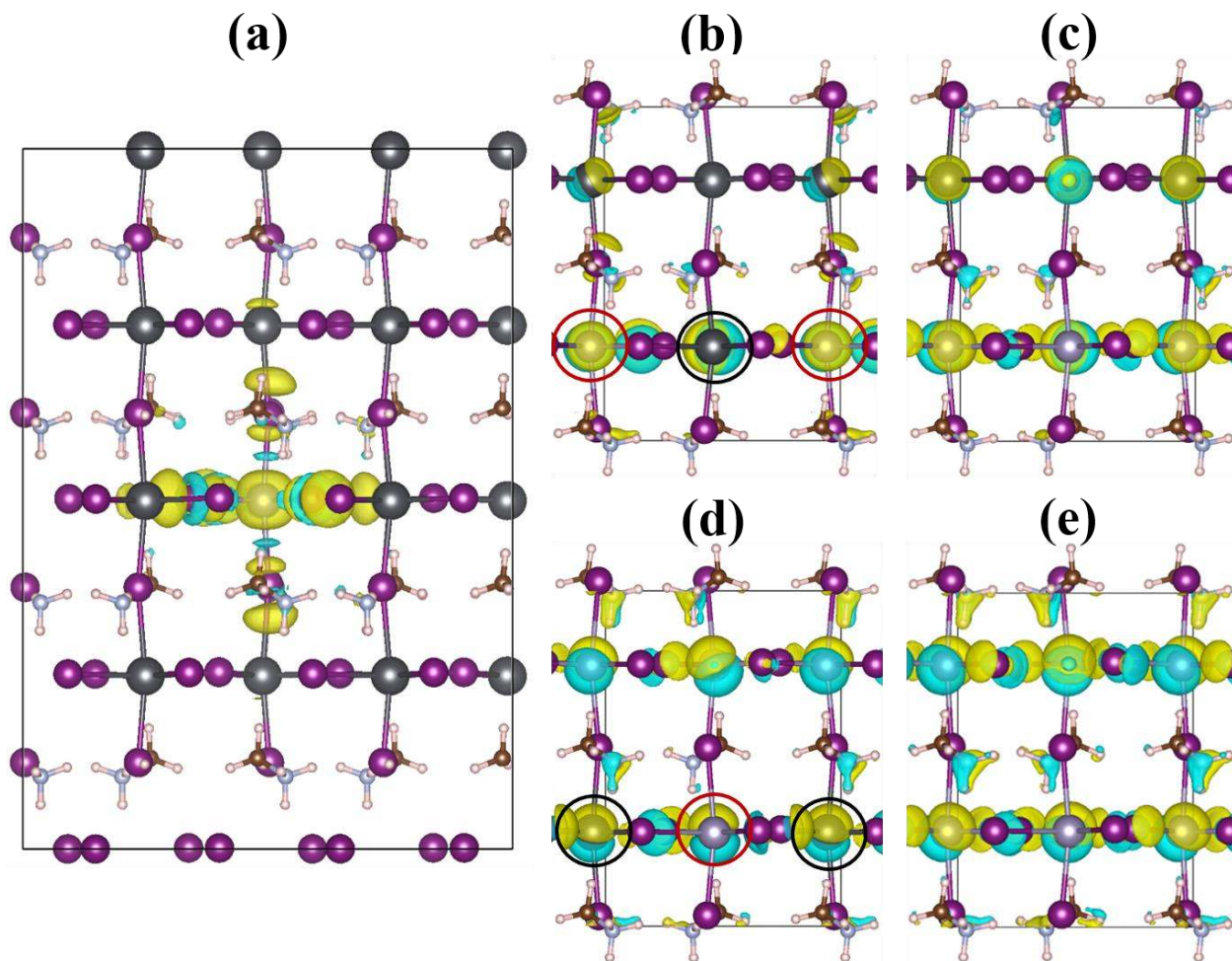
Figure 4. Charge density of hole polaron in (a) $MAPb_{0.97}Sn_{0.03}I_3$, (b) $MAPb_{0.75}Sn_{0.25}I_3$, (c) $MAPb_{0.50}Sn_{0.50}I_3$, (d) $MAPb_{0.25}Sn_{0.75}I_3$ and (e) $MASnI_3$. Highlighted red and black circle represent the Sn and Pb atom, respectively. Isosurface values of 0.001 e·Å^{-3} and 0.018 e·Å^{-3} have been used for the charge density plots of figures (a) and (b)-(d), respectively.

As in the case of MAPbI$_3$, the projections of ions cartesian displacements upon the hole injection for all the mixed and full tin systems have been carried out (see Figure 5 and Figure S7-10 in Supporting Information). In all cases the injection of the hole leads to the activation of low energy Pb-I and Sn-I bending modes (<80 cm^{-1}, see Figure S11). Moreover, in the case of mixed Pb-Sn systems the emergence of new higher energy phonon modes at 110.1 cm^{-1}, 110.7 cm^{-1} and

108.1 cm^{-1} have been found for $MAPb_{0.75}Sn_{0.25}I_3$ and $MAPb_{0.50}Sn_{0.50}I_3$ and $MAPb_{0.25}Sn_{0.75}I_3$ systems, respectively. These modes are activated in the metal-iodide stretching region (see Figure S12). However, the coupling strength gradually decreases with increasing Sn concentration from $MAPb_{0.75}Sn_{0.25}I_3$ to $MAPb_{0.25}Sn_{0.75}I_3$, whereas these high energy stretching modes are completely absent in the symmetrical structure of $MAPbI_3$ and $MASnI_3$ and thus indicating a typical nature in mixed Pb-Sn systems, which is likely related to the asymmetric relaxation of the lattice responsible of polaron localization. It is noteworthy to mention that the peak at 129 cm^{-1}, 130 cm^{-1} and 136 cm^{-1} in $MAPbI_3$, $MAPb_{0.75}Sn_{0.25}I_3$ and $MAPb_{0.50}Sn_{0.50}I_3$, respectively arises due to the rotation of molecule and bending of Pb-I bonds.
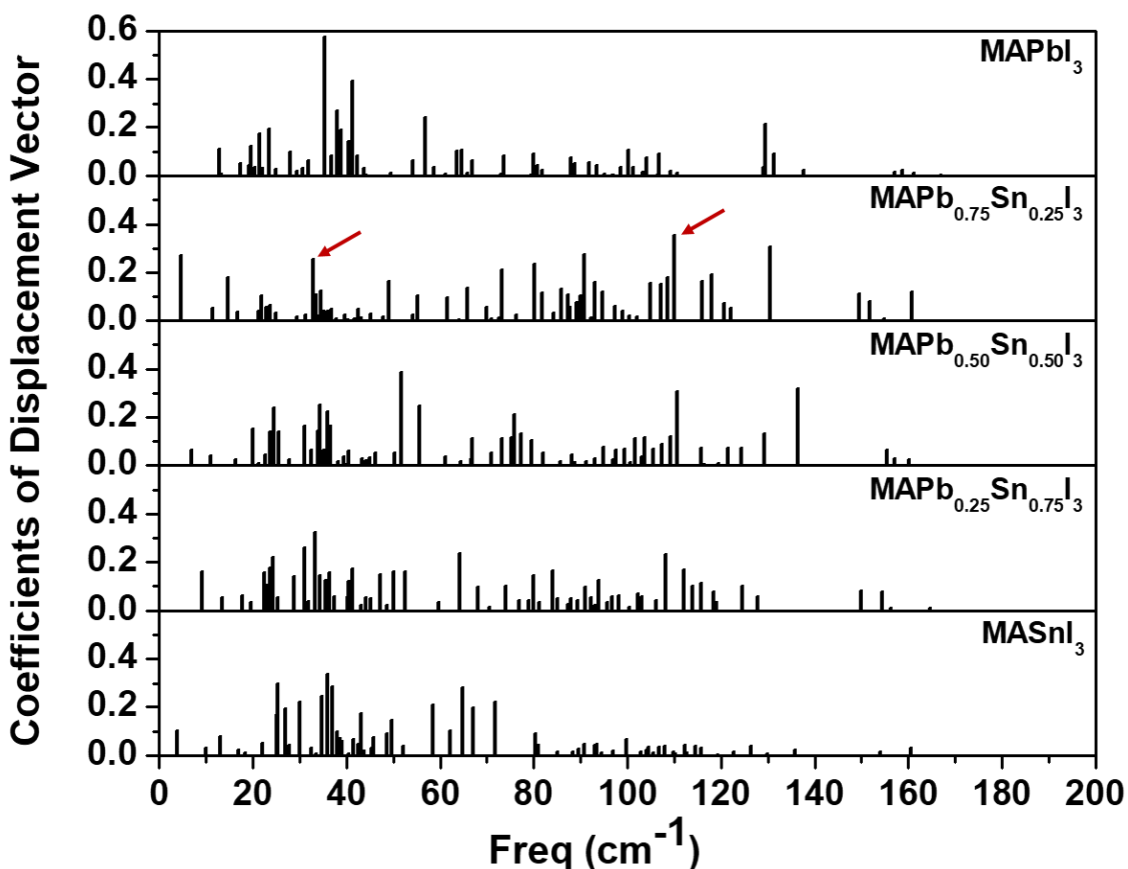
Figure 5. Coefficients of the displacement vector associated with a positive charge injection. Strong signals represent the strongly-coupled phonon modes to the displacement. The high energy stretching modes are activated in $MAPb_{0.75}Sn_{0.25}I_3$ and $MAPb_{0.50}Sn_{0.50}I_3$, whereas low energy bending modes are activated in the other cases. The red arrows in $MAPb_{0.75}Sn_{0.25}I_3$ indicates the bending and stretching modes and the specific atomic motions have been shown in Figure S11 and S12 in Supporting Information.

In summary, we have systematically studied the influence of the chemical composition of the perovskite on the polaron properties in metal halides ABX_3 perovskites by means of state of the art ab initio calculations. By varying the A-site cations (FA, MA, Cs and Cs:MA), B-site cations (Pb, Sn and Pb:Sn) and X-site anions (Br, I), we find that the stronger structural distortions occur for Cs than for MA and FA, with the effect of different A-site cations being almost additive. For the same A-cation, bromide shows stronger distortions than iodide perovskites. On the other hand, the pure Sn phase has an almost double polaron stabilization energy compared to the pure Pb phase. Surprisingly, the trend of polaron stabilization energy is non monotonic in mixed Sn:Pb perovskites, having the maximum for small Sn percentages. Polaron formation is found to be attributed to bond asymmetry, i.e the short-long nature of the metal-halide bonds, ranging from small to large polarons with the increasing Sn percentage in mixed Sn:Pb perovskites.

Author Information:

Corresponding Authors
*E-mail: arup.mahata@iit.it (A.M)
*E-mail: daniele.meggiolaro@iit.it (D.M.)

Acknowledgments:

Supporting Information:

The Supporting Information is available free of charge on the ACS Publications website.

Supporting information contains the computational details relying on the ref[54, 55, 66-70] (Text S1), experimental cell parameters taken from the ref[2, 42, 71-73] (Table S1), structural parameters of pure and mixed composition structures (Figure S1 and S4-S6), band gap and density of states of pure and mixed Pb-Sn structures (Table S2 and Figure S2), IR frequencies and coefficient of displacement vectors (Figure S7-S10 and S14-15), snapshot of the specific atomic motions for the bending and stretching modes of $MAPb_{0.75}Sn_{0.25}I_3$ (Figure S11-S12), electron polaron's charge density (Figure S13), hole polaron's density (Figure S16).

References:

1.   Green, M. A.; Ho-Baillie, A.; Snaith, H. J., The emergence of perovskite solar cells. *Nat. Photon.* **2014,** *8*, 506-514.
2.   Stoumpos, C. C.; Malliakas, C. D.; Kanatzidis, M. G., Semiconducting Tin and Lead Iodide Perovskites with Organic Cations: Phase Transitions, High Mobilities, and Near-Infrared Photoluminescent Properties. *Inorg. Chem.* **2013,** *52*, 9019-9038.
3.   Mosconi, E.; Amat, A.; Nazeeruddin, M. K.; Graetzel, M.; De Angelis, F., First-Principles Modeling of Mixed Halide Organometal Perovskites for Photovoltaic Applications. *J. Phys. Chem. C* **2013,** *117*, 13902−13913.
4.   Stranks, S. D.; Eperon, G. E.; Grancini, G.; Menelaou, C.; Alcocer, M. J. P.; Leijtens, T.; Herz, L. M.; Petrozza, A.; Snaith, H. J., Electron-Hole Diffusion Lengths Exceeding 1 Micrometer in an Organometal Trihalide Perovskite Absorber. *Science* **2013,** *342*, 341-344.

5.   Miyata, A.; Mitioglu, A.; Plochocka, P.; Portugall, O.; Wang, J. T.-W.; Stranks, S. D.; Snaith, H. J.; Nicholas, R. J., Direct measurement of the exciton binding energy and effective masses for charge carriers in organic-inorganic tri-halide perovskites. *Nat. Phys.* **2015,** *11*, 582-587.

6.   Wehrenfennig, C.; Eperon, G. E.; Johnston, M. B.; Snaith, H. J.; Herz, L. M., High Charge Carrier Mobilities and Lifetimes in Organolead Trihalide Perovskites. *Adv. Mater.* **2014,** *26*, 1584-1589.

7.   Srimath Kandada, A. R.; Petrozza, A., Photophysics of Hybrid Lead Halide Perovskites: The Role of Microstructure. *Acc. Chem. Res.* **2016,** *49*, 536-544.

8.   Poncé, S.; Schlipf, M.; Giustino, F., Origin of Low Carrier Mobilities in Halide Perovskites. *ACS Energy Lett.* **2019**, 456-463.

9.   Etienne, T.; Mosconi, E.; De Angelis, F., Dynamical Origin of the Rashba Effect in Organohalide Lead Perovskites: A Key to Suppressed Carrier Recombination in Perovskite Solar Cells? *J. Phys. Chem. Lett.* **2016,** *7*, 1638–1645.

10.   Kepenekian, M.; Robles, R.; Katan, C.; Sapori, D.; Pedesseau, L.; Even, J., Rashba and Dresselhaus Effects in Hybrid Organic–Inorganic Perovskites: From Basics to Devices. *ACS nano* **2015**.

11.   Liu, S.; Zheng, F.; Koocher, N. Z.; Takenaka, H.; Wang, F.; Rappe, A. M., Ferroelectric Domain Wall Induced Band Gap Reduction and Charge Separation in Organometal Halide Perovskites. *J. Phys. Chem. Lett.* **2015,** *6*, 693-699.

12.   Frost, J. M.; Butler, K. T.; Brivio, F.; Hendon, C. H.; van Schilfgaarde, M.; Walsh, A., Atomistic Origins of High-Performance in Hybrid Halide Perovskite Solar Cells. *Nano Lett.* **2014,** *14*, 2584-2590.

13.   Jankowska, J.; Prezhdo, O. V., Ferroelectric Alignment of Organic Cations Inhibits Nonradiative Electron–Hole Recombination in Hybrid Perovskites: Ab Initio Nonadiabatic Molecular Dynamics. *J. Phys. Chem. Lett.* **2017,** *8*, 812-818.

14.   Chen, Y.; Yi, H. T.; Wu, X.; Haroldson, R.; Gartstein, Y. N.; Rodionov, Y. I.; Tikhonov, K. S.; Zakhidov, A.; Zhu, X. Y.; Podzorov, V., Extended carrier lifetimes and diffusion in hybrid perovskites revealed by Hall effect and photoconductivity measurements. *Nat. Commun.* **2016,** *7*, 12253.

15.   Miyata, K.; Meggiolaro, D.; Trinh, M. T.; Joshi, P. P.; Mosconi, E.; Jones, S. C.; De Angelis, F.; Zhu, X.-Y., Large polarons in lead halide perovskites. *Sci. Adv.* **2017,** *3*, e1701217.

16.   Frohna, K.; Deshpande, T.; Harter, J.; Peng, W.; Barker, B. A.; Neaton, J. B.; Louie, S. G.; Bakr, O. M.; Hsieh, D.; Bernardi, M., Inversion symmetry and bulk Rashba effect in methylammonium lead iodide perovskite single crystals. *Nat. Commun.* **2018,** *9*, 1829.

17.   Zhang, X.; Shen, J.-X.; Wang, W.; Van de Walle, C. G., First-Principles Analysis of Radiative Recombination in Lead-Halide Perovskites. *ACS Energy Lett.* **2018,** *3*, 2329-2334.

18.   Ivanovska, T.; Dionigi, C.; Mosconi, E.; De Angelis, F.; Liscio, F.; Morandi, V.; Ruani, G., Long-Lived Photoinduced Polarons in Organohalide Perovskites. *J. Phys. Chem. Lett.* **2017**, 3081-3086.

19.   Neukirch, A. J.; Nie, W.; Blancon, J.-C.; Appavoo, K.; Tsai, H.; Sfeir, M. Y.; Katan, C.; Pedesseau, L.; Even, J.; Crochet, J. J.; et al. Polaron Stabilization by Cooperative Lattice Distortion and Cation Rotations in Hybrid Perovskite Materials. *Nano Lett.* **2016,** *16*, 3809-3816.

20.   Park, M.; Neukirch, A. J.; Reyes-Lillo, S. E.; Lai, M.; Ellis, S. R.; Dietze, D.; Neaton, J. B.; Yang, P.; Tretiak, S.; Mathies, R. A., Excited-state vibrational dynamics toward the polaron in methylammonium lead iodide perovskite. *Nat. Commun.* **2018,** *9*, 2525.

21.   Neukirch, A. J.; Abate, I. I.; Zhou, L.; Nie, W.; Tsai, H.; Pedesseau, L.; Even, J.; Crochet, J. J.; Mohite, A. D.; Katan, C.; et al. Geometry Distortion and Small Polaron Binding Energy Changes with Ionic Substitution in Halide Perovskites. *J. Phys. Chem. Lett.* **2018,** *9*, 7130-7136.

22.   Sendner, M.; Nayak, P. K.; Egger, D. A.; Beck, S.; Müller, C.; Epding, B.; Kowalsky, W.; Kronik, L.; Snaith, H. J.; Pucci, A.; et al. Optical phonons in methylammonium lead halide perovskites and implications for charge transport. *Mater. Horiz.* **2016,** *3*, 613-620.

23.   Yin, J.; Li, H.; Cortecchia, D.; Soci, C.; Brédas, J.-L., Excitonic and Polaronic Properties of 2D Hybrid Organic–Inorganic Perovskites. *ACS Energy Lett.* **2017,** *2*, 417-423.

24.	Cortecchia, D.; Yin, J.; Bruno, A.; Lo, S.-Z. A.; Gurzadyan, G. G.; Mhaisalkar, S.; Brédas, J.-L.; Soci, C., Polaron self-localization in white-light emitting hybrid perovskites. *J. Mater. Chem. C* **2017,** *5*, 2771-2780.

25.	Yin, J.; Maity, P.; De Bastiani, M.; Dursun, I.; Bakr, O. M.; Brédas, J.-L.; Mohammed, O. F., Molecular behavior of zero-dimensional perovskites. *Sci. Adv.* **2017,** *3*, e1701793.

26.	Zhu, X. Y.; Podzorov, V., Charge Carriers in Hybrid Organic–Inorganic Lead Halide Perovskites Might Be Protected as Large Polarons. *J. Phys. Chem. Lett.* **2015,** *6*, 4758-4761.

27.	Diab, H.; Trippé-Allard, G.; Lédée, F.; Jemli, K.; Vilar, C.; Bouchez, G.; Jacques, V. L. R.; Tejeda, A.; Even, J.; Lauret, J.-S.; et al. Narrow Linewidth Excitonic Emission in Organic–Inorganic Lead Iodide Perovskite Single Crystals. *J. Phys. Chem. Lett.* **2016,** *7*, 5093-5100.

28.	Zhu, H.; Trinh, M. T.; Wang, J.; Fu, Y.; Joshi, P. P.; Miyata, K.; Jin, S.; Zhu, X. Y., Organic Cations Might Not Be Essential to the Remarkable Properties of Band Edge Carriers in Lead Halide Perovskites. *Adv. Mater.* **2017,** *29*, 1603072.

29.	Evans, T. J. S.; Miyata, K.; Joshi, P. P.; Maehrlein, S.; Liu, F.; Zhu, X. Y., Competition Between Hot-Electron Cooling and Large Polaron Screening in CsPbBr3 Perovskite Single Crystals. *J. Phys. Chem. C* **2018,** *122*, 13724-13730.

30.	Ambrosio, F.; Wiktor, J.; De Angelis, F.; Pasquarello, A., Origin of low electron–hole recombination rate in metal halide perovskites. *Energy Environ. Sci.* **2018,** *11*, 101-105.

31.	Zhu, H.; Miyata, K.; Fu, Y.; Wang, J.; Joshi, P. P.; Niesner, D.; Williams, K. W.; Jin, S.; Zhu, X.-Y., Screening in crystalline liquids protects energetic carriers in hybrid perovskites. *Science* **2016,** *353*, 1409-1413.

32.	Price, M. B.; Butkus, J.; Jellicoe, T. C.; Sadhanala, A.; Briane, A.; Halpert, J. E.; Broch, K.; Hodgkiss, J. M.; Friend, R. H.; Deschler, F., Hot-carrier cooling and photoinduced refractive index changes in organic–inorganic lead halide perovskites. *Nat. Commun.* **2015,** *6*, 8420.

33.	Niesner, D.; Zhu, H.; Miyata, K.; Joshi, P. P.; Evans, T. J. S.; Kudisch, B. J.; Trinh, M. T.; Marks, M.; Zhu, X. Y., Persistent Energetic Electrons in Methylammonium Lead Iodide Perovskite Thin Films. *J. Am. Chem. Soc.* **2016,** *138*, 15717-15726.

34.	Guo, Z.; Wan, Y.; Yang, M.; Snaider, J.; Zhu, K.; Huang, L., Long-range hot-carrier transport in hybrid perovskites visualized by ultrafast microscopy. *Science* **2017,** *356*, 59.

35.	Chen, K.; Barker, A. J.; Morgan, F. L. C.; Halpert, J. E.; Hodgkiss, J. M., Effect of Carrier Thermalization Dynamics on Light Emission and Amplification in Organometal Halide Perovskites. *J. Phys. Chem. Lett.* **2015,** *6*, 153-158.

36.	Yang, Y.; Ostrowski, D. P.; France, R. M.; Zhu, K.; van de Lagemaat, J.; Luther, J. M.; Beard, M. C., Observation of a hot-phonon bottleneck in lead-iodide perovskites. *Nat. Photon.* **2015,** *10*, 53.

37.	Frost, J. M.; Whalley, L. D.; Walsh, A., Slow Cooling of Hot Polarons in Halide Perovskite Solar Cells. *ACS Energy Lett.* **2017,** *2*, 2647-2652.

38.	Zheng, F.; Wang, L.-w., Large polaron formation and its effect on electron transport in hybrid perovskites. *Energy Environ. Sci.* **2019**.

39.	Wang, Z.; Lin, Q.; Chmiel, F. P.; Sakai, N.; Herz, L. M.; Snaith, H. J., Efficient ambient-air-stable solar cells with 2D–3D heterostructured butylammonium-caesium-formamidinium lead halide perovskites. *Nat. Energy* **2017,** *2*, 17135.

40.	Ju, D.; Dang, Y.; Zhu, Z.; Liu, H.; Chueh, C.-C.; Li, X.; Wang, L.; Hu, X.; Jen, A. K. Y.; Tao, X., Tunable Band Gap and Long Carrier Recombination Lifetime of Stable Mixed CH3NH3PbxSn1–xBr3 Single Crystals. *Chem. Mater.* **2018,** *30*, 1556-1565.

41.	Pisanu, A.; Mahata, A.; Mosconi, E.; Patrini, M.; Quadrelli, P.; Milanese, C.; De Angelis, F.; Malavasi, L., Exploring the Limits of Three-Dimensional Perovskites: The Case of FAPb1–xSnxBr3. *ACS Energy Lett.* **2018,** *3*, 1353-1359.

42.   Hao, F.; Stoumpos, C. C.; Chang, R. P. H.; Kanatzidis, M. G., Anomalous Band Gap Behavior in Mixed Sn and Pb Perovskites Enables Broadening of Absorption Spectrum in Solar Cells. *J. Am. Chem. Soc.* **2014,** *136*, 8094-8099.

43.   Eperon, G. E.; Leijtens, T.; Bush, K. A.; Prasanna, R.; Green, T.; Wang, J. T.-W.; McMeekin, D. P.; Volonakis, G.; Milot, R. L.; May, R.; et al. Perovskite-perovskite tandem photovoltaics with optimized band gaps. *Science* **2016,** *354*, 861-865.

44.   Goyal, A.; McKechnie, S.; Pashov, D.; Tumas, W.; Schilfgaarde, M. v.; Stevanović, V., Origin of Pronounced Nonlinear Band Gap Behavior in Lead–Tin Hybrid Perovskite Alloys. *Chem. Mater.* **2018,** *30*, 3920-3928.

45.   Im, J.; Stoumpos, C. C.; Jin, H.; Freeman, A. J.; Kanatzidis, M. G., Antagonism between Spin–Orbit Coupling and Steric Effects Causes Anomalous Band Gap Evolution in the Perovskite Photovoltaic Materials CH3NH3Sn1–xPbxI3. *J. Phys. Chem. Lett.* **2015,** *6*, 3503-3509.

46.   Galkowski, K.; Surrente, A.; Baranowski, M.; Zhao, B.; Yang, Z.; Sadhanala, A.; Mackowski, S.; Stranks, S. D.; Plochocka, P., Excitonic Properties of Low Bandgap Lead-Tin Halide Perovskites. *ACS Energy Lett.* **2019**.

47.   Abate, A., Perovskite Solar Cells Go Lead Free. *Joule* **2017,** *1*, 659-664.

48.   Leijtens, T.; Prasanna, R.; Bush, K. A.; Eperon, G. E.; Raiford, J. A.; Gold-Parker, A.; Wolf, E. J.; Swifter, S. A.; Boyd, C. C.; Wang, H.-P.; et al. Tin–lead halide perovskites with improved thermal and air stability for efficient all-perovskite tandem solar cells. *Sustainable Energy Fuels* **2018,** *2*, 2450-2459.

49.   Yang, Z.; Rajagopal, A.; Chueh, C.-C.; Jo, S. B.; Liu, B.; Zhao, T.; Jen, A. K. Y., Stable Low-Bandgap Pb–Sn Binary Perovskites for Tandem Solar Cells. *Adv. Mater.* **2016,** *28*, 8990-8997.

50.   Cho, H.; Jeong, S.-H.; Park, M.-H.; Kim, Y.-H.; Wolf, C.; Lee, C.-L.; Heo, J. H.; Sadhanala, A.; Myoung, N.; Yoo, S.; et al. Overcoming the electroluminescence efficiency limitations of perovskite light-emitting diodes. *Science* **2015,** *350*, 1222-1225.

51.   Ling, Y.; Yuan, Z.; Tian, Y.; Wang, X.; Wang, J. C.; Xin, Y.; Hanson, K.; Ma, B.; Gao, H., Bright Light-Emitting Diodes Based on Organometal Halide Perovskite Nanoplatelets. *Adv. Mater.* **2016,** *28*, 305-311.

52.   Yantara, N.; Bhaumik, S.; Yan, F.; Sabba, D.; Dewi, H. A.; Mathews, N.; Boix, P. P.; Demir, H. V.; Mhaisalkar, S., Inorganic Halide Perovskites for Efficient Light-Emitting Diodes. *J. Phys. Chem. Lett.* **2015,** *6*, 4360-4364.

53.   Leyden, M. R.; Meng, L.; Jiang, Y.; Ono, L. K.; Qiu, L.; Juarez-Perez, E. J.; Qin, C.; Adachi, C.; Qi, Y., Methylammonium Lead Bromide Perovskite Light-Emitting Diodes by Chemical Vapor Deposition. *J. Phys. Chem. Lett.* **2017,** *8*, 3193-3198.

54.   Perdew, J. P.; Ernzerhof, M.; Burke, K., Rationale for mixing exact exchange with density functional approximations. *J. Chem. Phys.* **1996,** *105*, 9982-9985.

55.   Perdew, J. P.; Burke, K.; Ernzerhof, M., Generalized Gradient Approximation Made Simple. *Phys. Rev. Lett.* **1996,** *77*, 3865-3868.

56.   Umari, P.; Mosconi, E.; De Angelis, F., Relativistic GW calculations on $CH_3NH_3PbI_3$ and $CH_3NH_3SnI_3$ Perovskites for Solar Cell Applications. *Sci. Rep.* **2014,** *4*, 4467.

57.   Meggiolaro, D.; De Angelis, F., First-Principles Modeling of Defects in Lead Halide Perovskites: Best Practices and Open Issues. *ACS Energy Lett.* **2018,** *3*, 2206-2222.

58.   Erhart, P.; Klein, A.; Åberg, D.; Sadigh, B., Efficacy of the DFT + U formalism for modeling hole polarons in perovskite oxides. *Phys. Rev. B* **2014,** *90*, 035204.

59.   Welch, E.; Scolfaro, L.; Zakhidov, A., Density functional theory + U modeling of polarons in organohalide lead perovskites. *AIP Adv.* **2016,** *6*, 125037.

60.   Quarti, C.; Grancini, G.; Mosconi, E.; Bruno, P.; Ball, J. M.; Lee, M. M.; Snaith, H. J.; Petrozza, A.; Angelis, F. D., The Raman Spectrum of the $CH_3NH_3PbI_3$ Hybrid Perovskite: Interplay of Theory and Experiment. *J. Phys. Chem. Lett.* **2013,** *5*, 279-284.

61.   Ma, J.; Wang, L.-W., Nanoscale Charge Localization Induced by Random Orientations of Organic Molecules in Hybrid Perovskite CH3NH3PbI3. *Nano Lett.* **2015,** *15*, 248-253.

62.   Even, J.; Pedesseau, L.; Katan, C., Analysis of Multivalley and Multibandgap Absorption and Enhancement of Free Carriers Related to Exciton Screening in Hybrid Perovskites. *J. Phys. Chem. C* **2014,** *118*, 11566-11572.

63.   Dastidar, S.; Li, S.; Smolin, S. Y.; Baxter, J. B.; Fafarman, A. T., Slow Electron–Hole Recombination in Lead Iodide Perovskites Does Not Require a Molecular Dipole. *ACS Energy Lett.* **2017,** *2*, 2239-2244.

64.   Hutter, E. M.; Savenije, T. J., Thermally Activated Second-Order Recombination Hints toward Indirect Recombination in Fully Inorganic CsPbI3 Perovskites. *ACS Energy Lett.* **2018,** *3*, 2068-2069.

65.   Kawai, H.; Giorgi, G.; Marini, A.; Yamashita, K., The Mechanism of Slow Hot-Hole Cooling in Lead-Iodide Perovskite: First-Principles Calculation on Carrier Lifetime from Electron–Phonon Interaction. *Nano Lett.* **2015,** *15*, 3103-3108.

66.   Giannozzi, P.; Baroni, S.; Bonini, N.; Calandra, M.; Car, R.; Cavazzoni, C.; Ceresoli, D.; Guido, L. C.; Cococcioni, M.; Dabo, I.; et al. QUANTUM ESPRESSO: a modular and open-source software project for quantum simulations of materials. *J. Phys.: Condens. Matter* **2009,** *21*, 395502.

67.   VandeVondele, J.; Krack, M.; Mohamed, F.; Parrinello, M.; Chassaing, T.; Hutter, J., Quickstep: Fast and accurate density functional calculations using a mixed Gaussian and plane waves approach. *Comput. Phys. Commun.* **2005,** *167*, 103-128.

68.   Goedecker, S.; Teter, M.; Hutter, J., Separable dual-space Gaussian pseudopotentials. *Phys. Rev. B* **1996,** *54*, 1703-1710.

69.   VandeVondele, J.; Hutter, J., Gaussian basis sets for accurate calculations on molecular systems in gas and condensed phases. *J. Chem. Phys.* **2007,** *127*, 114105.

70.   Guidon, M.; Hutter, J.; VandeVondele, J., Auxiliary Density Matrix Methods for Hartree−Fock Exchange Calculations. *J. Chem. Theory Comput.* **2010,** *6*, 2348-2364.

71.   Niemann, R. G.; Gouda, L.; Hu, J.; Tirosh, S.; Gottesman, R.; Cameron, P. J.; Zaban, A., Cs+ incorporation into CH3NH3PbI3 perovskite: substitution limit and stability enhancement. *J. Mater. Chem. A* **2016,** *4*, 17819-17827.

72.   Marronnier, A.; Roma, G.; Boyer-Richard, S.; Pedesseau, L.; Jancu, J.-M.; Bonnassieux, Y.; Katan, C.; Stoumpos, C. C.; Kanatzidis, M. G.; Even, J., Anharmonicity and Disorder in the Black Phases of Cesium Lead Iodide Used for Stable Inorganic Perovskite Solar Cells. *ACS Nano* **2018,** *12*, 3477-3486.

73.   Chung, I.; Song, J.-H.; Im, J.; Androulakis, J.; Malliakas, C. D.; Li, H.; Freeman, A. J.; Kenney, J. T.; Kanatzidis, M. G., CsSnI$_3$: Semiconductor or Metal? High Electrical Conductivity and Strong Near-Infrared Photoluminescence from a Single Material. High Hole Mobility and Phase-Transitions. *J. Am. Chem. Soc.* **2012,** *134*, 8579-8587.